Helmholtz-Zentrum
Geesthacht
Zentrum für Material- und Küstenforschung

Original

Kostov, V.; Gibmeier, J.; Wilde, F.; Staron, P.; Roessler, R.; Wanner, A.:

Fast in situ phase and stress analysis during laser surface treatment: A synchrotron x-ray diffraction approach

In: Review of Scientific Instruments (2012) AIP

DOI: 10.1063/1.4764532

Fast *in situ* phase and stress analysis during laser surface treatment: A synchrotron x-ray diffraction approach

V. Kostov,[1] J. Gibmeier,[1,a)] F. Wilde,[2] P. Staron,[2] R. Rössler,[1] and A. Wanner[1]
[1]*Institute of Applied Materials (IAM-WK), Karlsruhe Institute of Technology, Karlsruhe 76131, Germany*
[2]*Institute of Materials Research, Helmholtz-Zentrum Geesthacht (HZG), Geesthacht 21502, Germany*

(Received 16 August 2012; accepted 13 October 2012; published online 5 November 2012)

An *in situ* stress analysis by means of synchrotron x-ray diffraction was carried out during laser surface hardening of steel. A single exposure set-up that based on a special arrangement of two fast silicon strip line detectors was established, allowing for fast stress analysis according to the $\sin^2\psi$ x-ray analysis method. For the *in situ* experiments a process chamber was designed and manufactured, which is described in detail. First measurements were carried out at the HZG undulator imaging beamline (IBL, beamline P05) at the synchrotron storage ring PETRA III, DESY, Hamburg (Germany). The laser processing was carried out using a 6 kW high power diode laser system. Two different laser optics were compared, a Gaussian optic with a focus spot of ø 3 mm and a homogenizing optic with a rectangular spot dimension of 8 × 8 mm^2. The laser processing was carried out using spot hardening at a heating-/cooling rate of 1000 K/s and was controlled via pyrometric temperature measurement using a control temperature of 1150 °C. The set-up being established during the measuring campaign allowed for this first realization data collection rates of 10Hz. The data evaluation procedure applied enables the separation of thermal from elastic strains and gains unprecedented insight into the laser hardening process. © *2012 American Institute of Physics*. [http://dx.doi.org/10.1063/1.4764532]

I. INTRODUCTION

Laser surface hardening is a processing technique aiming to improve the material properties of the near-surface regions of steel components. It produces hard, wear resistant surface layers by means of a local heat treatment provoking a ferrite-austenite transformation followed by martensite formation.[1,2] The required local heating is accomplished by the use of high power laser radiation as energy source, while the subsequent rapid cooling is due to self-quenching of the material combined with controlled laser heating. Due to the interaction between the laser beam photons and the free electrons at the workpiece surface the laser beam is absorbed within an area, which lateral dimensions are limited by the laser beam cross section size.[3] The beam absorption causes a transformation of the laser photon energy in thermal energy, which induces a process-related thermal cycle at the top material surface with maximal processing temperatures between the austenite phase transformation temperature A_3 and the melting temperature T_m. Power densities at the work-piece surface above 10^4 W/cm^2 allow for very short interaction times, allowing to reach the maximal processing temperature within less than a second.[4,5] The temperature course at the surface determines the temperature evolution in the depth via thermal conduction within the workpiece. The local irradiation area and the short processing time cause a local heating only in the near surface areas. Upon heating the surface region above the A_3 temperature, a ferrite-austenite phase transformation (α-γ) takes place. In comparison with a slow heating, the A_3 temperature during the laser heat treatment is shifted to higher temperatures as consequence of the higher heating rates and due to the rather short time for carbon-diffusion into the austenite nuclei.[6,7] Due to high rate of heat transfer, steep temperature gradients between the heated process area and the base material, which remains non-affected by the laser treatment, arise, which result in rapid cooling by conduction. This causes the transformation of the austenitised surface layers to martensite (α') below the martensite start temperature M_s without the need for external quenching. This self-quenching occurs as the cold interior of the work-piece constitutes a sufficiently large heat sink to quench the hot surface at a rate high enough to prevent ferrite-pearlite or bainite formation inside of the processed region, resulting in a hard martensite structure with material hardness up to 1000 HV and hardening depths up to 1.7 mm depending on the process parameters applied.[8–10] According to literature an increase in the cooling rate up to 3000 K/s does not effect a significant change in the M_s temperature for austenizing temperatures above 1000 °C.[7] The γ–α' phase transformation, which is accompanied by significant shear and volume strain in combination with the different thermal strain states of the processed region and the bulk material lead to the generation of characteristic compressive residual stresses inside of the martensitic transformed zone after cooling down to room temperature. These are compensated by tensile residual stresses outside of the laser affected area.[11] Compared to conventional hardening processes local laser surface hardening results in much lower distortion of the components.[4,5]

In recent time laser-hardening has gained in popularity that can be associated with the development of high-performance diode-laser systems due to their outstanding

a)Author to whom correspondence should be addressed. Electronic mail: Jens.Gibmeier@kit.edu.

 © 2012 American Institute of Physics

Downloaded 03 Jul 2013 to 141.4.208.26. This article is copyrighted as indicated in the abstract. Reuse of AIP content is subject to the terms at: http://rsi.aip.org/about/rights_and_permissions

characteristics, e.g., their compact design, the rectangular intensity distribution in the focal-spot, or the low wavelength.[3] The latter one results in a larger absorption of the beam intensity in contrast to Nd-YAG or CO_2-lasers which leads, e.g., coating free heat treatment and/or to higher heating rates. Modern high-power-diode-lasers (HPDLs) can be operated by means of optical fiber-coupling which makes them attractive for the integration in production processes due to their high degree of flexibility.

Although many studies were conducted in the field of laser-hardening (e.g., Refs. 1, 2, and 8–11) the underlying evolutions of microstructure and strains are still not well understood. The optimization of laser surface hardening processes has so far largely been based on correlating process parameters to post-treatment properties and residual stress states of the component.[11–17]

A large step towards a deeper process understanding can be reached if a real-time insight into the complex and fast thermo-mechanical processes during laser surface hardening can be obtained. As will be shown in the following, synchrotron-based x-ray diffraction offers a viable approach. X-ray diffraction has many times been shown to allow *in situ* studies of technical processes like spot welding,[18–20] arc welding,[21] or heat treatment by mean of furnace stage.[22–24] All of the cited studies aimed at the analyses of phase transformations and/or of the changes of the d-spacing, but in neither of these studies thermal and elastic strains were separated. In Rocha and Hirsch[25] an advanced method was applied to study also the stress evolutions during fast heat treatment processes "quasi" *in situ*: The stress evolutions during austenisation and during gas quenching of steel samples were studied using an area detector according to the $\sin^2\psi$ method. However, in order to provide the required variation in the ψ-tilts, repeated measurement were carried out for several samples processed in the same fashion, but analyzed at different ψ-angles.

In this work, an approach for time resolved lattice diffraction, which allows for the instant separation of thermal and elastic strains, has been established and adapted to the requirements of laser surface hardening of steels using a HPDL system. In the following, the experimental set-up, the experimental procedures, and the data evaluation strategy are explained in detail. Laser surface hardening of steel type AISI 4140 for heating-/cooling rates of 1000 K/s was applied with two different laser optics, a 3 mm diameter Gaussian optic and a 8×8 mm^2 homogenizing optic. The results of the phase- and strain-/stress-evolution are carefully discussed with respect to results of supplementary microstructural analysis and *ex situ* x-ray stress analysis in the final state after laser surface hardening.

II. EXPERIMENTAL SET-UP FOR TIME RESOLVED X-RAY DIFFRACTION ANALYSIS DURING LASER SURFACE HARDENING

A. Methodical approach/data collection and evaluation

The general idea of the diffraction set-up is based on early work by Macherauch and Müller[26] who established a single exposure technique for x-ray stress analysis according to the $\sin^2\psi$-method using film exposures. With the newest generation of fast silicon strip line detectors this approach can be used for time resolved x-ray stress analysis during rapid processes. In Kostov *et al.*[27] and Altenkirch *et al.*[28] we have demonstrated this for rapid heat treatment processes as well as during gas tungsten arc welding of steels. In the present study, the experimental set-up has been adapted for laser surface hardening using a specifically designed process chamber, which provides laser radiation protection and vacuum or inert gas atmosphere. The latter is required for preventing oxidizing process during laser hardening[29] and thus for an appropriate process control via pyrometric temperature measurement. The instrumentation is described in detail in Sec. II B.

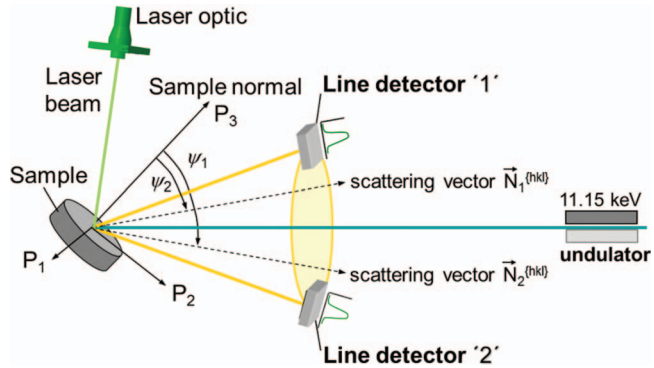

FIG. 1. Schematic of the experimental set-up for synchrotron x-ray stress analysis during laser surface treatment. Two line detectors are positioned at different ψ positions, allowing stress analysis according to the $\sin^2\psi$ method.

Two line detectors are positioned in the backscatter range ($2\theta \gg 90°$) symmetrically to the primary synchrotron beam, as shown schematically in Figure 1. The two detectors record diffraction spectra from the same diffraction cones, hence they give redundant diffraction data for fast phase analysis. However, the data are non-redundant for stress analysis if the sample surface is tilted with respect to the primary synchrotron x-ray beam. The specimen tilting results in two different distant angles ψ, which are defined as the angles between the scattering vector N and the normal to the samples surface P_3. In the present study, the photon energy was set to 11.15 keV (corresponding to a photon wavelength of $\lambda = 0.111\,21$ nm) and a fixed specimen tilt of 35° was used, resulting in $\psi_1 = 16.9°$ and $\psi_2 = 53.1°$ for the ferrite diffraction peaks and $\psi_1 = 13.3°$ and $\psi_2 = 36.0°$ for the austenite diffraction peaks. Consequently, using this two-detector approach, two data points in the 2θ vs. $\sin^2\psi$-plot can be plotted for a particular diffraction peak.

For data analysis various post treatments had to be carried out prior to the diffraction line fitting. First a flat field correction of the diffraction data was carried out for the individual detector modules according to Schmitt *et al.*,[30] aiming to equalize the different detector channel efficiencies. The flat field image was obtained by long-term flat illumination of the detector modules using diffracted intensity of an amorphous glass plate and identical measuring parameters as for the diffraction analysis on the steel samples. The flat field correction was followed by a background correction of the measuring data and an absorption correction. Subsequently, the diffraction lines were fitted using a Pearson VII function.

Downloaded 03 Jul 2013 to 141.4.208.26. This article is copyrighted as indicated in the abstract. Reuse of AIP content is subject to the terms at: http://rsi.aip.org/about/rights_and_permissions

The further data treatment enables the separation between in-plane thermal and elastic strains, since the slopes of the 2θ vs. $\sin^2\psi$ lines are due to elastic strains only whereas the vertical shifts of the lines are caused by thermal strains or changes of the chemical phase composition.

In the first step the 2θ vs. $\sin^2\psi$ lines determined for each process time/step i were extrapolated to $\sin^2\psi = 1$, hence the surface parallel strain component was evaluated. The elastic lattice strain $\epsilon_{el,,i}^{\{hkl\}}$ was calculated on the basis of the slope of the individual fit lines of the 2θ vs. $\sin^2\psi$ distributions, according to

$$\varepsilon_{el,i}^{\{hkl\}} = -\frac{1}{2}\theta_i^*(2\theta_i - 2\theta_i^*) \quad (1)$$

taking into account the $2\theta^*$-value for the strain free direction ψ^* that again can be calculated for the assumption of a biaxial stress state with $\sigma_{33} = 0$ by

$$\sin^2\psi^* = -2\,s_1^{\{hkl\}}/1/2s_2^{\{hkl\}}. \quad (2)$$

ψ^* was extracted from the fit lines of 2θ vs. $\sin^2\psi$. $s_1^{\{hkl\}}$ and $1/2s_2^{\{hkl\}}$ are the diffraction elastic constants (DEC) for the individual diffraction lines of type {hkl}. The thermal strains $\varepsilon_{th,i}^{\{hkl\}}$ are calculated by the parallel shifts of the 2θ vs. $\sin^2\psi$-fit lines, with

$$\varepsilon_{th,i}^{\{hkl\}} = -\frac{1}{2}\theta_{RT}^*(2\theta_i^* - 2\theta_{RT}^*). \quad (3)$$

Figure 2 illustrates as an example the data evaluation for the applied two detector single exposure set-up only for the heating-up phase of the laser hardening experiment. On the right hand side the temperature-time evolution during heating up is shown for the same experiment. The diagram on the left hand side shows the evaluated peak positions in the center of the process zone during heating up to a temperature of 700 °C for selected data points of the {422}-ferrite interference line measured with the two line detector modules ($2\Theta_1$ and $2\Theta_2$) at the two different ψ angles. $\psi*$ indicate the stress free direction. The 2θ vs. $\sin^2\psi$ fit lines show vertical shifts caused by the thermal expansion of the material and changes in the slope due to stresses arising from constraint from the surrounding (cold) material.

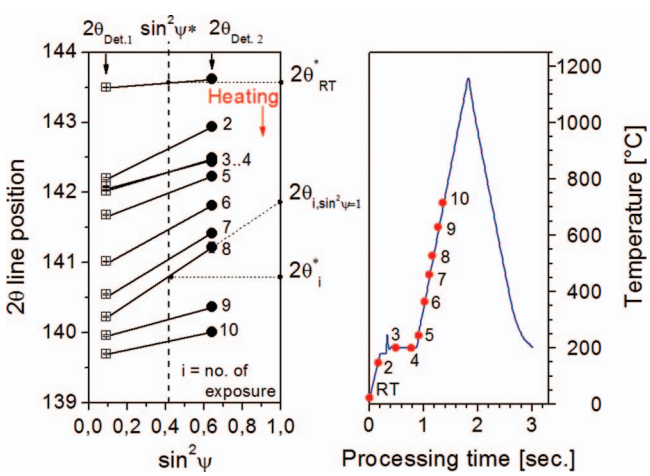

FIG. 2. Illustration of the data evaluation for the first data points during heating up of the material due to the local heat input by means of the high power laser beam.

B. Instrumentation

The set-up consists of (i) the diode laser system with pyrometric process control, (ii) the process chamber, (iii) the detector system, and (iv) a monochromatic x-ray source with sufficiently high photon flux in the soft x-ray regime. Once the experimental set-up has been mounted and aligned with respect to the synchrotron x-ray beam, no further translational or rotational movement of any component is required for the measurements. Hence, no diffractometer is needed.

1. Synchrotron x-ray beamline

The *in situ* experiments during laser hardening of steels were carried out at the HZG (Helmholtz-Zentrum Geesthacht) imaging beamline (IBL; beamline P05) at the synchrotron storage ring PETRA III at DESY, Hamburg (Germany).[31,32] The energy range at beamline P05 is tunable between 5 and 50 keV by means of a liquid nitrogen cooled, fixed exit double crystal monochromator (DCM) equipped with silicon single crystals (111) and (311) designed by DESY. Using this DCM very high monochromatization ($\Delta E/E \approx 10^{-4}$) can be achieved. For applications which need particularly high flux (e.g., fast *in situ* experiments) a double multilayer monochromator (DMM) equipped with different flat and bent substrates is currently under construction ($\Delta E/E$ up to 10^{-2}). The laser hardening experiment was installed in the second experimental hutch (EH2), which is located in a distance of approximately 83 m to the undulator source. The photon flux after the monochromator accounts for approx. 3×10^{13} Ph/(s/mm^2) at a photon energy of 10 keV. This is the only requirement for the choice of a suitable synchrotron beamline for a successful implementation of the approach. The beamline must offer a sufficient photon flux density for soft X-radiation between 7–12 keV at a relative large beam cross section up to approx. 1×1 mm^2 and sufficient space to host the mobile process chamber with the adapters for the laser optic and the pyrometer for temperature control as well as the integrated line detector modules. No diffractometer is required since the set-up remains stationary once the whole set-up has been positioned on the axis of the synchrotron x-ray beam.

2. Diode laser system

For laser hardening a fiber coupled 6 kW high power diode laser system of type LDF 6000-60 from Laserline GmbH, Mülheim-Kärlich (Germany) was used. Two different laser hardening optics were applied alternatively: a homogenizing optic with a spot size of 8×8 mm^2 and an optic with a nominal diameter of the focused laser beam of ø 3 mm, which could be easily exchanged by means of a patented adapter at the end of the laser fiber. For the pyrometric temperature control of the laser hardening process a one-color (monochromatic) pyrometer from Dr. Mergenthaler GmbH & Co.KG, Neu-Ulm (Germany) was used. The laser hardening process was controlled using the LASCON software from Mergenthaler. The pyrometer PC was linked with the laser system control unit that was located in the experimental hutch of the synchrotron beamline P05. The access to the

Downloaded 03 Jul 2013 to 141.4.208.26. This article is copyrighted as indicated in the abstract. Reuse of AIP content is subject to the terms at: http://rsi.aip.org/about/rights_and_permissions

laser control unit from the control hutch of P05 was granted using the remote software LL-Control from Laserline GmbH. The pyrometer limits the process parameter window for laser surface hardening since its sensitive temperature range is between 180 and 1500 °C. Thus the control of the process starts and ends at the lower pyrometer limit of 180 °C.

3. Process chamber

The optics of the laser system was mounted to the process chamber, which was designed and manufactured at the Institute of Applied Materials (IAM-WK). A photograph of the process chamber is presented in Figure 3(a). The close-up view (Figure 3(b)) shows the interior of the chamber. As stated above, the process chamber is required for laser protection and for a reliable process control, which can only be guaranteed in the absence of surface oxidization affecting the pyrometric temperature measurement. Thus, the chamber was equipped with a vacuum option to evacuate the chamber before flooding it by an inert gas flow at a slight overpressure of approximately 0.25 bar. Helium is used as inert gas since it shows a lower attenuation of soft X-radiation in contrast to, e.g., Argon and since pre-studies indicated excellent process controllability under Helium atmosphere.[29] The process chamber is based on a cylindrical tube with outer diameter 215 mm and length 380 mm, with removable covers at both end faces (see Figure 3), which are dedicated for maintenance as well as for sample exchange. The diameter of the chamber and the wall thickness were dimensioned by calculation of the heat load that might appear in a worst case scenario for pure reflexion of the intense laser beam at a minimum focus of ø 2.8 mm and a continuous laser power output of 1.5 kW, which was expected to be the most critical parameter choice from the process parameter window for technical relevant laser surface hardening processes of steel. This condition the chamber wall has to withstand for a time period of 100 s. As material austenitic stainless steel and a wall thickness of 2.5 mm was used. For security reasons the temperature at the inner wall of the chamber is measured at critical positions and the laser process is immediately aborted if the temperature exceeds 80 °C, which was never the case in all tests carried out.

The cylindrical chamber offers the possibility to couple in the laser beam by means of a coated glass window, which has a transmission of >99.9% for the continuous (cw) wavelength of the laser system that is between 910 and 1040 nm depending on the diode stacks activated. The laser optic is mounted on a support that allows for a manual adjustment of the laser focus.

A similar support is used for mounting and for the adjustment of the focus of the pyrometer. The pyrometer radiation is transmitted from the laser treated sample via a glass window with a transmission of >99% for the wavelength range 1650–2000 nm. The adjustment of the pyrometer is carried out using an integrated low energy (class 2) pilot laser with a wavelength of 640 nm. For the fine adjustment of the laser beam, i.e., to ensure that synchrotron beam, pyrometer axis and laser beam intercept in one point at the center of the process chamber, the pilot laser (class 1) of the diode laser system is used. Both, the pyrometer window and the diode laser window are equipped with water cooling. The primary synchrotron beam enters and leaves the chamber via a 10 mm wide slit, which is sealed by a polyimide foil (Kapton®) with a thickness of 75 μm glued directly to the chamber wall using epoxy adhesive. The slit has a length that covers a range in 2θ from 120° to 175° symmetrical to the primary beam. The specimen stage inside the process chamber provides translation perpendicular to the sample surface (z-axis translation) and in the direction parallel to the specimen surface and transverse to the synchrotron beam (x-axis translation). These translational movements allow fine adjustment of the sample in the center of the chamber. In addition, the x-axis translation allows line-hardening along a path length of up to 100 mm. The axes for sample manipulation are dimensioned for a maximum sample weight of 500 g. For reproducible alignment

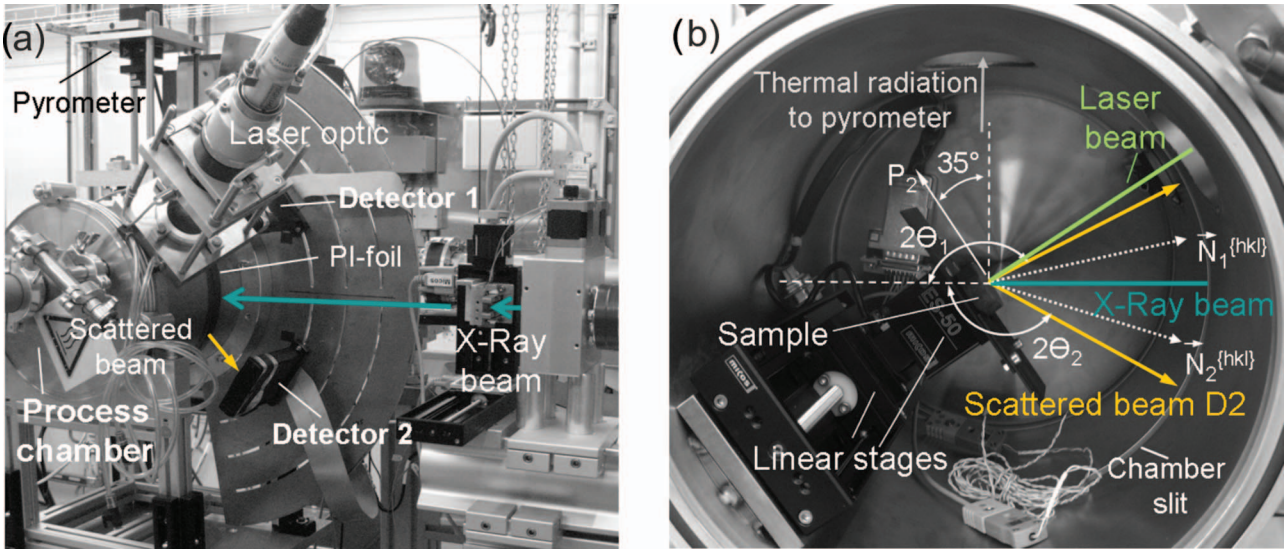

FIG. 3. Process chamber designed for on-line diffraction studies during laser surface hardening. (a) Overview of the closed chamber with the arrangement of the two detector set-up used. (b) View inside the process chamber, showing the sample stage with the translation axis for fine adjustment of the sample.

Downloaded 03 Jul 2013 to 141.4.208.26. This article is copyrighted as indicated in the abstract. Reuse of AIP content is subject to the terms at: http://rsi.aip.org/about/rights_and_permissions

of the sample in the chamber center a small mechanical dial gauge is used, which can be mounted on a small optical track at the inside of the chamber. In total the chamber including all necessary technical components like detector modules, pyrometer, laser optic has a weight of approximately 35 kg and is thus easily transferrable to and from any experimental station of any synchrotron radiation facility.

4. Detector system

Line detector modules of type Mythen 1K from Dectris Ltd., Baden (Switzerland) are used for recording of the diffraction spectra. The read-out time of these detectors is 250 μs and the count rate is 1 MHz per channel. The sensitive area of the line detector module is a silicon sensor with 1280 8-mm long stripes with a pitch of 50 μm and a thickness of 300 μm, thus covering a detector length of 64 mm. The modules were directly mounted at the chamber on a wing (see Fig. 1) parallel to the diffraction plane (vertical direction). The wing provides three concentric grooves with distances to the sample surface of 200, 250 and 300 mm for detector positioning in the backscatter range. The basic idea is to adjust the detector module pairs symmetrically to the primary beam to record diffraction spectra from the same diffraction cone but at different tilt angles, since the sample is pre-tilt (here: pre-tilt = 35°). In this case, the two detector modules were adjusted at a distance to the sample of 200 mm, which gave a good compromise between attenuation and angular resolution. Thus, the coverage in 2θ was about 18° for each of the detector modules. The detector were positioned with the mid position at approximately $2\theta = 143°$ to monitor the shift of the {422}-diffraction lines of the ferrite / martensite phase with $2\theta_{\alpha/\alpha'} = 143.7°$and to allow for the detection of the {600}-austenite diffraction line with $2\theta_{\gamma} = 136.6°$ at the chosen photon energy of 11.15 keV ($\lambda = 0.111\,21$ nm). For data evaluation the angular positions of the detector modules has to be determined in order to assign a correct 2θ-angle to the channel number of the line detector. This was accomplished using LaB_6 powder as calibration substance, which shows various diffraction lines in the 2θ-range covered by the two line detector modules. Further, Fe-powder was used to give a direct calibration (stress free position) of the ferrite/martensite diffraction line studied. As stated before, various data post treatments had to be carried out prior to the diffraction line fitting.

III. PROCESS PARAMETERS FOR LASER SURFACE HARDENING

As explained in Sec. II B 2 two different laser optics were compared for surface laser hardening of steel AISI 4140, a Gaussian optic with a focus spot of ø 3 mm and a homogenizing optic with a nominal rectangular spot dimension of 8 × 8 mm^2. The laser processing was carried out using spot hardening at a heating-/cooling rate of 1000 K/s and was controlled via pyrometric temperature measurement using a control temperature of 1150 °C. The temperature-time evolution of the applied surface hardening process is shown in Figure 4 for each of the laser optics used. The surface hardening was

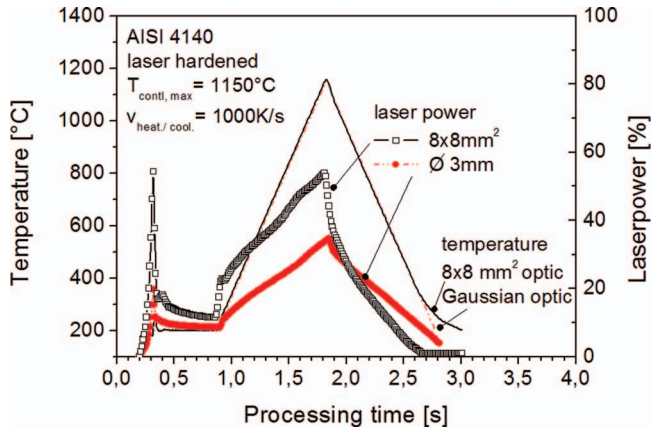

FIG. 4. Laser power used to achieve the defined temperature vs. process time course for the two optics applied for laser hardening. Data from LASCON software used for pyrometric process control.

carried out in helium atmosphere in order to prevent surface oxidation and to guarantee a good thermal condition through the inert gas atmosphere. Furthermore, Figure 4 indicates the laser power that is needed to achieve the pre-defined heating and cooling rate. Only part of the total power of nominal 6 kW of the high power diode laser system is needed for an appropriate process control, i.e., about 55% in case of the large homogenizing optic and only about 33% for the ø 3 mm Gaussian optic. The over compensation in the beginning of the laser surface treatment is due to the applied one-color pyrometer, which is only sensitive in the working temperature range from 180 °C up to 1500 °C.

For the *in situ* synchrotron x-ray studies an x-ray beam with a cross section of 0.8 × 0.8 mm^2 was used for the analyses of the laser surface hardening with the ø 3 mm Gaussian optic. For the sample pre-tilt about 35° the surface region illuminated by the synchrotron x-ray beam covers an area of approximately 0.8 × 0.9 mm^2. For the application of the 8 × 8 mm^2 homogenizing optic a slightly larger cross section of the synchrotron beam with 1.2 × 1.2 mm^2 was used in order to gain statistics. Here, the region illuminated by the synchrotron x-ray beam amounts to approximately 1.2 × 1.4 mm^2. Thus, using the larger optics a gain in counting statistics by a factor of approximately 2.3 was realized.

IV. EXEMPLARY LASER-HARDENING STUDY

A. Material and microstructure

Heat treatable steel AISI 4140 (German grade: 42 CrMo 4) in a quenched and tempered state was used as testing material. Cylindrical samples of dimension ø 25 mm × 10 mm were produced. One circular face of each sample was ground mechanically aiming to guarantee a reproducible surface quality with similar laser absorption and thermal emission grades. Subsequently, a stress relief heat treatment was carried out at 550 °C for 90 min in vacuum to provide a ´stress free´ state as starting condition for the laser treatment and the *in situ* diffraction stress analyses. Figure 5 shows micrographs of the process zones obtained upon laser treatment for the two optics applied: (a) Gaussian optic with 3 mm spot

Downloaded 03 Jul 2013 to 141.4.208.26. This article is copyrighted as indicated in the abstract. Reuse of AIP content is subject to the terms at: http://rsi.aip.org/about/rights_and_permissions

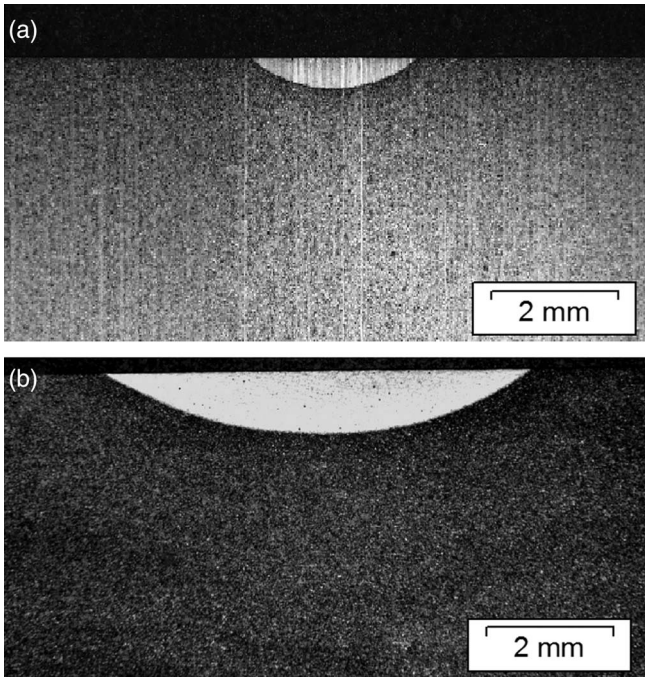

FIG. 5. Micrograph of the process zone (overview) after laser surface hardening using (a) a Gaussian optic with 3 mm diameter and (b) a homogenizing optic with a spot size of 8 × 8 mm^2.

diameter and (b) homogenizing optic with square spot dimension of 8 × 8 mm^2. In Figure 6 the corresponding cross-sections of the laser-treated regions are presented. In both cases, a half lens-shaped process zone is obtained, the dimensions of which are primarily governed by the laser spot and heat input. Similar microstructures are obtained in both cases, showing a martensitic microstructure (mixed martensite), which is in accordance to observations from literature using the same material.[10]

Figure 7 shows the Martens hardness (HM) measured on the cross-section in a distance of 30 μm to the surface at a test load of 300 mN using a Vickers pyramid according to the testing standard EN ISO 14577.[33] The micro-hardness distribution at the very surface reflects the lateral dimension of the focus of the applied laser optic. The martensitic hardened zone is much harder (about 6700 HM) than the unaffected base material (about 3700 HM). No significant difference in

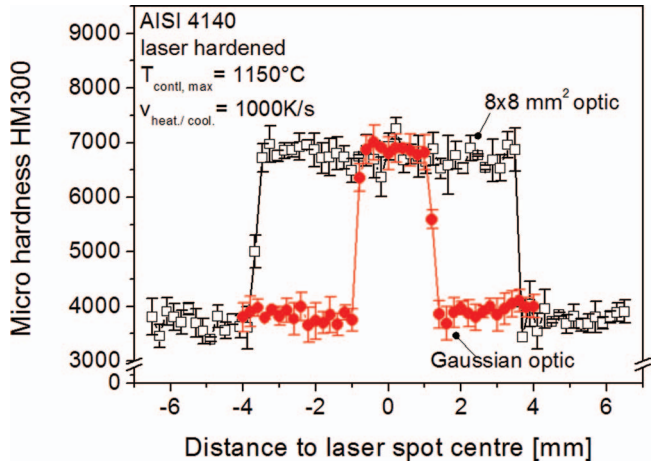

FIG. 7. Comparison of the micro-hardness distribution at the cross-sectional plane in lateral direction in a distance of 30 μm to the surface of the laser hardened samples for different laser optics applied.

the resulting hardness levels can be observed between the two laser optics applied.

B. Spatial resolved residual stress analysis (*ex situ* studies)

In addition to the microstructural analysis the local residual stresses were determined following the laser processing. X-ray residual stress analysis according to the $\sin^2\psi$-method was applied for the {211}-interference line of α-ferrite/martensite (α') using V-filtered CrKα-radiation. As primary aperture a pinhole collimator with a nominal diameter of 0.5 mm was applied. In front of the scintillation counter a symmetrizing slit[34] was applied. 13 sample tilts between $-60^\circ < \psi < 60^\circ$ with equidistant steps in $\sin^2\psi$ were used. For stress evaluation the DEC, $s_1^{\{211\}} = -1.27 \cdot 10^{-6}\,\mathrm{MPa}^{-1}$ and $1/2s_2^{\{211\}} = 5.82 \cdot 10^{-6}\,\mathrm{MPa}^{-1}$, are used. The diagram in Figure 8 indicates that for both optics a W-shaped distribution of the surface residual stress is obtained. Inside the process zone the residual stresses are compressive, outside the process zone they are tensile, decaying to zero with increasing distance from the heat treated zone. The absolute values of residual stress reach much higher levels for the 8 × 8 mm^2 spot laser optic than for the 3 mm diameter spot optic. On

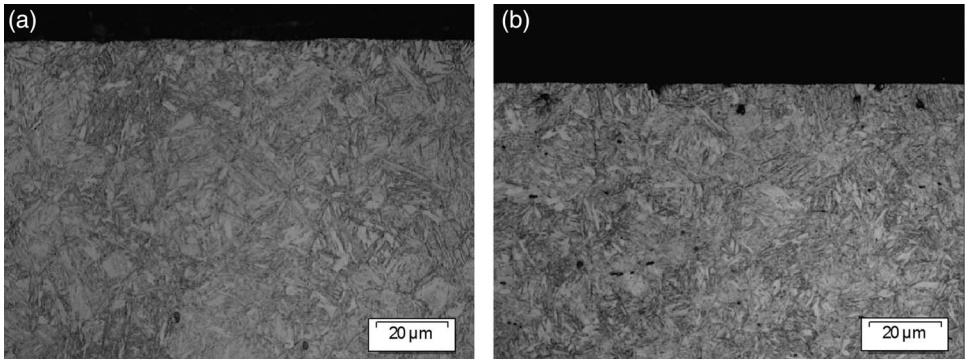

FIG. 6. Micrograph of the center of the process zone (detail at near surface region) after laser surface hardening using (a) a Gaussian optic with 3 mm diameter, or (b) a homogenizing optic with a spot size of 8 × 8 mm^2.

Downloaded 03 Jul 2013 to 141.4.208.26. This article is copyrighted as indicated in the abstract. Reuse of AIP content is subject to the terms at: http://rsi.aip.org/about/rights_and_permissions

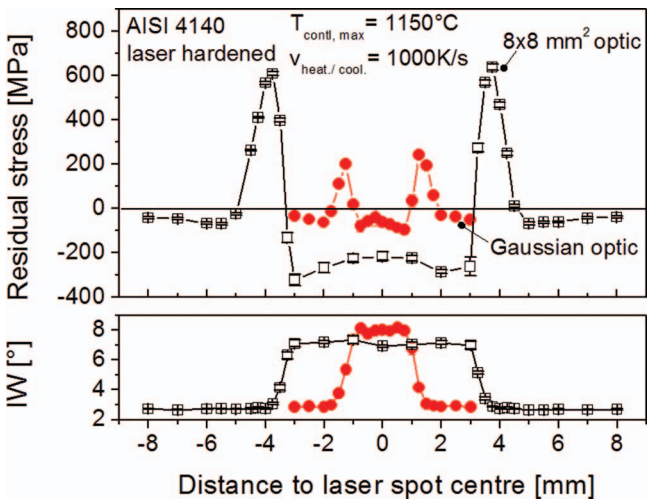

FIG. 8. Comparison of the distribution of the residual stress (upper diagram) and of the integral widths (IW, lower diagram) of the diffraction lines at the surface of the laser hardened samples for different laser optics applied after laser processing.

the other hand, the integral widths (IW) of the interference lines, which are a measure for the work hardening induced, are slightly higher in the zone processed using the 3 mm diameter spot optic.

C. Results and discussion of *in situ* analyses during laser hardening

1. Temperature-time depended phase transformations

Synchrotron x-ray diffraction test measurements on laser treated steel samples indicated that the martensite peaks are quite broad and weak, thus limiting the sampling rate of x-ray detection to 10 Hz in all process steps in which martensite is present. Thus, throughout the *in situ* experiments of the present study, the sampling rate was set to 10 Hz, and each diffraction measurement obtained during heating or cooling at a rate of ±1000 K/s is an average over a specimen surface temperature interval of 100 K. The temperatures reported in the following are the center values of these intervals. In Figure 9 the diffraction spectra during laser surface hardening are plotted versus the processing time as 2D-contour plots. The corresponding temperature evolutions in the center of the laser spot as measured by the monochromatic pyrometer are also shown in these diagrams. The difference in net counts of the diffraction intensity observed between the two experiments can be attributed to the smaller cross sectional area of the synchrotron beam applied in the laser hardening experiment using the 3 mm diameter Gaussian laser beam optic. The temperature evolutions in the spot centers are similar for both laser optics, except for the cooling at the end of the process. Below the temperature of 380 °C the temperature-time curve for the 8 × 8 mm^2 homogenizing optic shows a clearly slower cooling rate due to the higher total heat input applied to this sample, which reduces the self-quenching rate to less than 1000 K/s.

Starting the laser heating, the sample surface first reaches a temperature of 200 °C, which is approx. the starting temperature of the monochromatic pyrometer (T_{start} = 180 °C). The sudden temperature increase results in a distinct shift of the {422}-α-ferrite interference lines at a process time of 0.3 s.

In the further course of the laser processing, which starts at a process time of 0.8 s (heating rate: 1000 K/s), the continuously increasing heat input results in a continuous shift of the ferrite interference line towards lower 2θ-angles, for both the detector modules. Further, a continuous decrease of the diffracted intensity can be noticed for increasing surface temperatures. Due to the higher counting statistic for the slightly larger cross section area of the synchrotron beam when using the 8 × 8 mm^2 homogenizing optic (Fig. 9(b)) one more diffraction spectrum (at a temperature of at 709 °C) can be recorded in contrast to the Gaussian optic (Fig. 9(a)) before the diffraction signal vanishes. Further, as a consequence of the limited length of the line detectors the $\alpha-\gamma$-transformation, which is expected during heating up at 793 °C for AISI 4140[10], and the strain evolution of the austenite phase during heating could not been recorded during the online diffraction studies. The latter is due to the large material expansion of the austenite at high temperatures that results in a large 2θ peak shift.

During cooling, the first austenite ($\gamma-$Fe) diffraction line enters the 2θ-range covered by the line detector at a surface temperature of (599 ± 50) °C for application of the

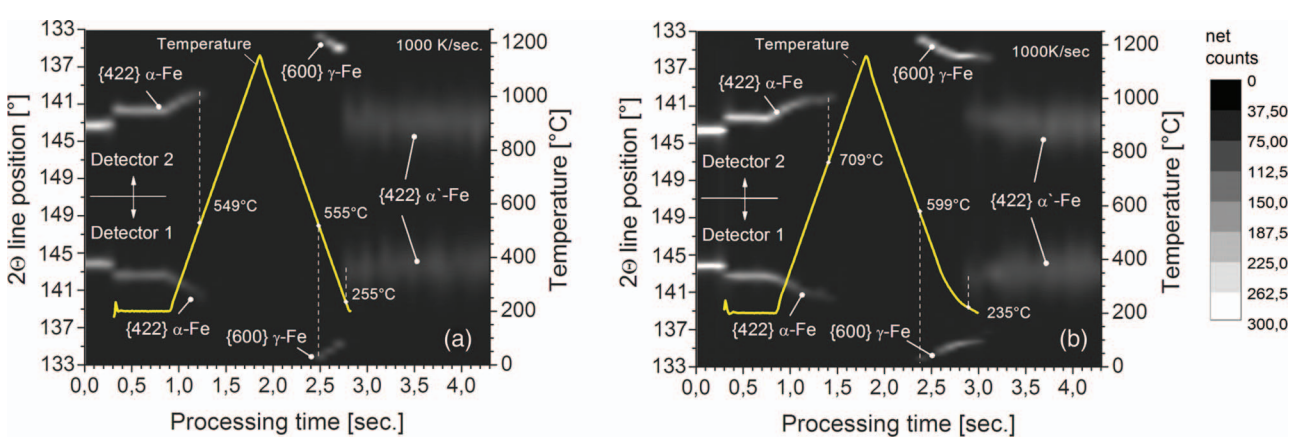

FIG. 9. 2D-contour-plot of the interference profiles recorded by the two line detectors (detector 1 and 2) and plot of the temperature vs. processing time for (a) using the Gaussian optic with 3 mm diameter and (b) using the homogenizing optic with a spot size of 8 × 8 mm^2.

Downloaded 03 Jul 2013 to 141.4.208.26. This article is copyrighted as indicated in the abstract. Reuse of AIP content is subject to the terms at: http://rsi.aip.org/about/rights_and_permissions

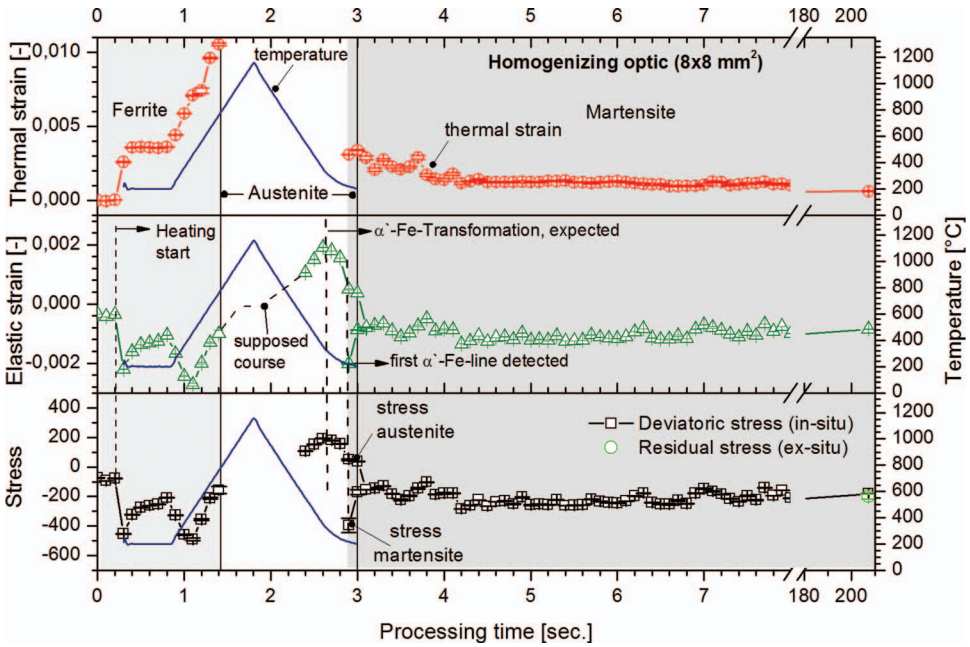

FIG. 10. Thermal strain (top), elastic strain (middle), and deviatoric stress component calculated from the elastic strain (bottom) vs. the processing time for local laser surface hardening of steel AISI 4140, using a homogenizing optic with a nominal spot size of 8 × 8 mm^2 with a heating/cooling rate of 1000 K/s and a control temperature of 1150 °C.

8 × 8 mm^2 homogenizing optic (see Fig. 9(b)). The further cooling of the process zone causes shifts of the diffraction line to higher 2θ values, as expected. The diffraction data clearly indicate the autenite-martensite transformation, which starts at about (255 ± 50) °C (3 mm diameter Gaussian optic, Fig. 9(a)) or at about (235 ± 50) °C (8 × 8 mm homogenizing optic, Fig. 9(b)). These martensite start (M_s) temperatures are significantly lower than the M_s temperatures of 380 °C or 340 °C reported in literature[10,12] that are obtained by dilatometer measurements on bulk samples subjected to similar heating/cooling cycles. Due to the higher counting statistic and / or the slower cooling rate when using the 8 × 8 mm^2 homogenizing optic (Fig. 9(b)) a martensite and an austenite diffraction lines can be recorded simultaneously at M_s and 0.1 s after martensite transformation at about (211 ± 50) °C. Upon cooling below 200 °C, only the interference line of the transformed martensite phase can be recorded for both optics applied. In previous *ex situ* studies a retained austenite fraction of less than 3% was determined, which is below the detection limit of the fast *in situ* diffraction setup.

2. Temperature-time dependent strain/stress evolution

The time-dependent evolution of the phase-specific thermal and elastic strains is presented for the homogenizing optic with a spot dimension of 8 × 8 mm^2 (Fig. 10) and for the 3 mm diameter Gaussian optic (Fig. 11), respectively. Further, the evolution of the near surface lateral deviatoric stress component is plotted versus the processing time. The stress was calculated from the elastic strain based on the assumption of a surface-parallel plane stress state, which is justified due to the small mean penetration depth of approximately 3 μm of soft x-rays at a photon energy of 11.15 keV and using diffraction elastic constants (DEC) that were calculated for the studied diffraction lines based on temperature dependent macroscopic elastic constants for the same steel grade from Graja.[35]

The strain and stress distributions indicate that the material is in slight compression at the start of the *in situ* diffraction experiment. Due to the local heat induction by means of the laser system the processing zone expands, but is constrained by the surrounding (cold) material, which results in a distinct increase in compressive elastic strain and stress at the beginning of the process.

During the following holding step at 200 °C the phase specific thermal strain does not change significantly. The same can be stated for the 3 mm diameter Gaussian optic. However, a difference can be observed for the course of the elastic strain/stress distribution during this holding step. While the course for the smaller 3 mm diameter optic is nearly constant a slightly decreasing compressive elastic strain/stress for a similar thermal strain evolution for the 8×8 mm^2 homogenizing optic (Figs. 10 and 11 as well as Fig. 12(b)) was determined. The divergences during that holding step at around 200 °C for the strain/stress distribution might be due to the larger laser spot size that results in a higher laser power applied and thus in a larger integral heat input. As a consequence, a rapid widening of the heated surface area occurs, which results in a kind of relaxation effect in the center of the process zone due to the decrease of the constraint given by the surrounded material.

The further heating results in a continuous increase in thermal strain. The direct comparison of the time dependent evolution (Fig. 12(a)) of the thermal strains for the two optics shows that during heating the courses are almost identical indicating that the pyrometric process control worked well even for the 3 mm diameter Gaussian optic since the focal diameter

Downloaded 03 Jul 2013 to 141.4.208.26. This article is copyrighted as indicated in the abstract. Reuse of AIP content is subject to the terms at: http://rsi.aip.org/about/rights_and_permissions

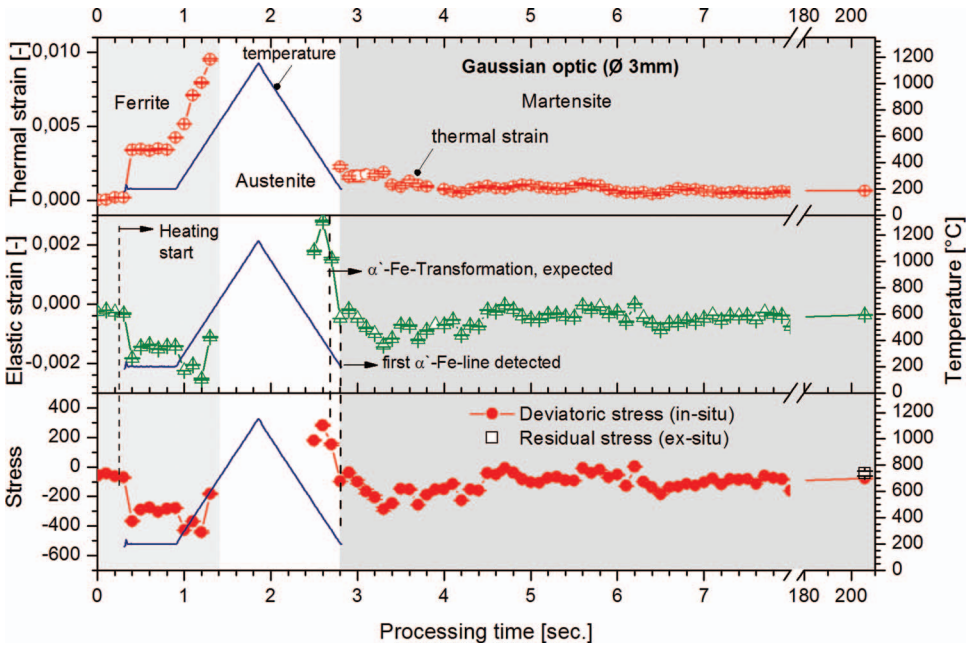

FIG. 11. Thermal strain (top), elastic strain (middle), and deviatoric stress component calculated from the elastic strain (bottom) vs. the processing time for local laser surface hardening of steel AISI 4140, using a 3 mm diameter Gaussian optic with a heating/cooling rate of 1000 K/s and a control temperature of 1150 °C.

of the pyrometer at the sample surface is approximately 2 mm in diameter.

As an effect of the increasing thermal expansion of the processed region and due to the constraint given by the surrounding cold material, the compressive elastic strain and the deviatoric stress increase continuously up to a temperature of approx. 500 °C. Here a sudden change can be observed towards a strongly decreasing compressive stress/strain evolution despite a further material expansion. This stress relaxation is attributed to local plastic deformations that occur due to a strong reduction of the yield strength for compression at higher temperatures. According to Nürnberger[36] the stress in the ferrite phase of a similar heat treated material drops from approx. 440 MPa at 500 °C to 175 MPa at a temperature of 700 °C.

The distribution of the phase specific thermal strain after austenite transformation could not be determined due to the missing diffraction data for this time period and further due to the lack of knowledge of the strain free lattice parameter and hence the respective line position $2\theta^*_{\text{RT-}\gamma}$ for austenite at ambient temperature. This is different from the evaluation of the elastic strains and the calculation of the deviatoric stress components, since only changes in the slopes of the 2θ vs. $\sin^2\psi$ lines are evaluated. The first austenite diffraction lines recorded during cooling (quenching) indicate for both optics studied here that the in-plane elastic tensile strains become larger with continuously decreasing surface temperature. The origin for this evolution has to be understood as a counteraction of the surrounded material to the thermal shrinkage of the processing zone and is supported due to its previous elastic-plastic compression during heating–up cycles. We assume that during heating with the 3 mm diameter Gaussian optic the material in the process zone is subjected to a higher degree of plastic compression in contrast to the larger homogenizing optic. The plastic compression has to be compensated during subsequent quenching. The quenching process generally results in a plastic tension of the material that will lead to compressive residual stresses after cooling down to ambient temperature. Since the effect of the martensitic transformation is assumed to be comparable in terms of compressive stress induced for both optics, the higher compressive residual stress in case of the 8×8 mm^2 homogenizing optic is due to the larger elastic-plastic strain generated by the quenching effect.

After martensite transformation a sudden change from tensile elastic strains towards compressive elastic strains can be observed (Figs. 10 and 11). The effect is similar in magnitude for both optics applied (Fig. 12(b)). The γ-α,′-transformation is accompanied by a volume increase, which in combination with the not transformed surrounding material leads to the generation of compressive strains. This phase specific volume strain superimposes the tensile strain due to quenching in such a way that characteristic compressive global elastic strains generate.

The time dependent evolution of the IW of the diffraction lines are displayed in Figure 12(c) and can further be used for discussion of the results. The final IW of the martensitic phase is slightly higher for the samples treated using the 3 mm diameter Gaussian optic. Since during heating the results of IW and also for the thermal and elastic strains are almost identical for the slightly differing synchrotron beam cross sections the definite changes after martensitic transformation can be clearly assigned to a materials effect. At comparable diffraction conditions higher values of IW indicate a higher degree of work hardening induced by the laser process, i.e., a higher dislocation density. Thus, the higher integral widths of the diffraction lines might be an indication for a higher degree of plastic deformation induced as a consequence of the

Downloaded 03 Jul 2013 to 141.4.208.26. This article is copyrighted as indicated in the abstract. Reuse of AIP content is subject to the terms at: http://rsi.aip.org/about/rights_and_permissions

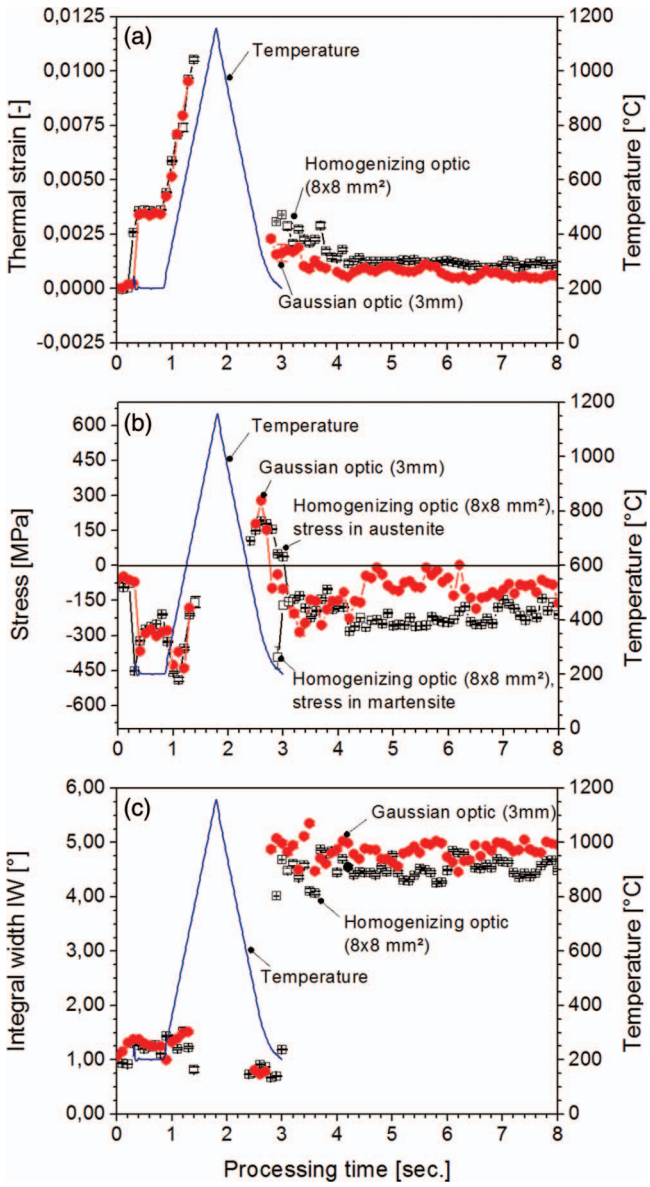

FIG. 12. Direct comparison of the thermal strain (a), the deviatoric stress (b), and the IW of the diffraction lines (c) vs. the processing time for laser surface hardening of steel AISI 4140 for the two different laser optics applied.

heating-up and/or quenching effect and further by the martensite transformation.

Upon cooling below the martensite finish temperature M_f no further materials volume expansion can be noticed by means of the diffraction data, moreover, the global elastic strain increases slightly. Upon cooling to room temperature compressive residual stresses are observed inside of the martensitic transformed region for both laser optics.

The *in situ* diffraction data reveal that after martensite transformation the compressive elastic strains for application of the 3 mm diameter Gaussian optic decrease continuously with increasing time, whilst for the application of the 8 $\times$ 8 mm^2 homogenizing optic they remain almost constant at a higher level. The stress fluctuations of approx. $\pm$75 MPa are result of the lower counting statistics. In the final state, upon cooling to room temperature, the compressive residual stresses in the process zone are clearly higher than compared to the optic that offers the smaller laser spot. The values at room temperatures are in good accordance with the residual stresses determined *ex situ* using a conventional lab x-ray source.

V. CONCLUSIONS

We proposed and established an experimental set-up and a data evaluation strategy for real-time monitoring of laser hardening of steels by means of synchrotron x-ray diffraction. The transportable set-up consists of a specially designed process chamber including a stage for sample manipulation, adaptations for the laser optic and the pyrometer for process control as well as a pair of line detectors that are positioned in the backscatter range. These detectors are attached directly at the process chamber and are adjusted to collect for diffraction line profiles of the same {hkl}-reflex, but at opposite positions of the Debye cone, thus allowing high-resolution strain analysis and the separation of elastic and thermal strains. The transportable set-up must be operated at a synchrotron soft x-ray beamline that offers a sufficient high photon flux for a relatively large cross sectional area of the x-ray beam in the range between 0.6 and 1.5 mm^2. First experiments were carried out at the HZG beamline P05@PETRA III (DESY, Hamburg, Germany) using a 6 kW HPDL system and two different laser optics, either a 3 mm diameter Gaussian optic or a homogenizing optic with a spot size of 8 $\times$ 8 mm^2. A case study was carried out for the laser hardening of steel AISI 4140.

The set-up realizes a simple single-exposure arrangement for the application of the $\sin^2\psi$-method of x-ray stress analysis thus allowing for fast *in situ* phase and stress analysis of the surface-near material under the assumption of a plane, surface-parallel stress state. The stress resolution was $\pm$75 MPa in the martensite phase and $\pm$35 MPa in the ferrite phase at a sampling rate of 10 Hz.

The first *in situ* diffraction experiments during laser hardening show that the size of the laser spot has a strong effect on the stress evolution as well as on the final residual stress state after laser hardening. Using the same temperature-time course for process control the smaller laser spot dimension results in much lower compressive residual stresses inside the process zone and as a consequence to much lower balancing tensile residual stresses at the edge of the process zone.

For the heating and cooling rate of $\pm$1000 K/s the time resolution of 100 ms corresponds to a resolution of 100 K per data point only. This limitation is, however, not due to the experimental set-up and in particular not due to the detector system applied, but is clearly caused by the limitation of the photon flux available and required for the analysis of the martensite phase (broad diffraction lines) for our first experiments. In order to achieve the desirable temperature resolution of 10–20 K in future experiments, the photon flux must be increased by a factor of 5 to 10 without increasing the spot size of the primary x-ray beam. At the used photon energy of 11.15 keV the x-ray absorption of air is a relevant factor. Hence, the experiment can be designed to minimize the gas absorption of the x-ray beam and thus to gain photon flux. This simple step will be immediately applied during

Downloaded 03 Jul 2013 to 141.4.208.26. This article is copyrighted as indicated in the abstract. Reuse of AIP content is subject to the terms at: http://rsi.aip.org/about/rights_and_permissions

future beamtimes. Furthermore, focusing optics may be used to enhance the flux in the observed area. Finally, with the installation of the DMM at P05 the photon flux will be much increased. Consequently, with these individual measures or better by a combination of them a photon flux enhancement of a factor of 5 seems feasible at beamline P05.

ACKNOWLEDGMENTS

We are grateful to BMBF for financial support through projects 05KS7VK1 and 05K10VKA. Further, we thank HZG for granting us beamtime at beamline P05@PETRA III. Special thank is given to Mr. Sidal from DESY, who supported the safety and radiation protection aspects during preparation and realization of the elaborate *in situ* experiment. Further we thank IAM-WK staff for contributing to the design and manufacturing of the process chamber and the technical staff of HZB for their excellent support at the beamline.

[1]K. Sridhar, V. A. Katkar, P. K. Singh, and J. M. Haake, Surf. Eng. **23**, 129 (2007).
[2]M. Heitkemper, A. Fischer, Ch. Bohne, and A. Pyzalla, Wear **250**, 477 (2001).
[3]F. Bachmann, W. Rath, and V. Auerbach, HTM **59**, 217 (2004).
[4]E. Kennedy, G. Byrne, and D. N. Collins, J. Mater. Process. Technol. **155–166**, 1855 (2004).
[5]J. C. Ion, Surf. Eng. **18**, 14 (2002).
[6]H. Schlicht, HTM **29**, 184 (1974).
[7]T. Miokovic, V. Schulze, D. Löhe, and O Vöhringer, HTM **59**, 304 (2003).
[8]H. W. Bergmann and E. Geissler, HTM **46**, 91 (1991).
[9]K. Obergfell, V. Schulze, and O. Vöhringer, Mater. Sci. Eng. **355**, 348 (2003).
[10]T. Miokovic, *Analyse des Umwandlungsverhalten bei ein- und mehrfacher Kurzzeithärtung bzw. Laserstrahlhärtung des Stahles 42CrMo4* (Shaker Verlag, Aachen, 2005).
[11]K. Müller, Doctor thesis, University Bayreuth, Bayreuth, 1999.
[12]N. S. Bailey, W. Tan, and Y. C. Shin, Surf. Coat. Technol. **203**, 2003 (2009).
[13]T. Miokovic, V. Schulze, O Vöhringer, and D. Löhe, Mater. Sci. Eng. A **435–436**, 547 (2006).
[14]R. Lin Peng and T. Ericsson, Scand. J. Metall. **27**, 223 (1998).
[15]K. Müller, C. Körner, and H. W. Bergmann, HTM **51**, 19 (1996).
[16]J. Domes, Doctor thesis, University Erlangen, Nürnberg, 1995.
[17]K. D. Schwager, B. Scholtes, and E. Macherauch, HTM **50**, 372 (1995).
[18]T. A. Palmer, J. W. Elmer, and S. S. Babu, Mater. Sci. Eng. A **374**, 307 (2004).
[19]S. S. Babu, J. W. Elmer, J. M. Vitec, and S. A. David, Acta Mater. **50**, 4763 (2002).
[20]J. W. Elmer, J. Wong, and T. Ressler, Scr. Mater. **43**, 751 (2000).
[21]H. Terasaki and Y. Komizo, Mater. Lett. **74**, 187 (2012).
[22]H. Terasaki, Y. Yamamoto, and Y. Komizo, Mater. Lett. **65**, 1745 (2011).
[23]H. Terasaki and Y. Komizo, Scr. Mater. **64**, 29 (2011).
[24]D. Zhang, H. Terasaki, and Y. Komizo, J. Alloys Compd. **484**, 929 (2009).
[25]A. d. S. Rocha and T. Hirsch, Mater. Sci. Eng. A **395**, 195 (2005).
[26]E. Macherauch and P. Müller, Z. Angew. Phys. **13**, 305 (1961).
[27]V. Kostov, J. Gibmeier, S. Doyle, and A. Wanner, Mater. Sci. Forum **638–642**, 2423 (2010).
[28]J. Altenkirch, J. Gibmeier, V. Kostov, A. Kromm, Th. Kannengiesser, S. Doyle, and A. Wanner, J. Strain Anal. Eng. Des. **46**(7), 563 (2011).
[29]V. Kostov, J. Gibmeier, and A. Wanner, "Laser surface hardening of steel: Effect of process atmosphere on the microstructure and residual stresses," Mater. Sci. Forum (in press).
[30]B. Schmitt, Ch. Bronnimann, and E. F. Eikenberry, Nucl. Instrum. Methods Phys. Res. A **518**, 436 (2004).
[31]A. Haibel, F. Beckmann, T. Dose, J. Herzen, M. Ogurreck, M. Müller, and A. Schreyer, Powder Diffr. **25**(2), 161 (2010).
[32]P. Staron, N. Schell, A. Haibel, F. Beckmann, T. Lippmann, L. Lottermoder, J. Herzen, T. Fischer, M. Kocak, and A. Schreyer, Mater. Sci. Forum **638–642**, 2470 (2010).
[33]DIN EN ISO 14577, *Instrumented Indentation Test for Hardness and Materials Parameters* (Beuth Verlag, Berlin, 2003).
[34]U. Wolfstieg, HTM **31**, 23 (1976).
[35]P. Graja, Doctor thesis, University of Karlsruhe, Karlsruhe, 1987.
[36]F. Nürnberger, Doctor thesis, University of Hanover, Hanover, 2010.

Downloaded 03 Jul 2013 to 141.4.208.26. This article is copyrighted as indicated in the abstract. Reuse of AIP content is subject to the terms at: http://rsi.aip.org/about/rights_and_permissions